PHYSICAL REVIEW C **103**, 064602 (2021)

Coupling dynamical and statistical mechanisms for baryonic cluster production in nucleus collisions of intermediate and high energies

A. S. Botvina,[1,2,3] N. Buyukcizmeci,[4] and M. Bleicher[1,3,5,6]
[1] *ITP J.W. Goethe University, D-60438 Frankfurt am Main, Germany*
[2] *Institute for Nuclear Research, Russian Academy of Sciences, 117312 Moscow, Russia*
[3] *Helmholtz Research Academy Hesse for FAIR (HFHF), GSI Helmholtz Center, Campus Frankfurt, Max-von-Laue-Strasse 12, 60438 Frankfurt am Main, Germany*
[4] *Department of Physics, Selcuk University, 42079 Konya, Turkey*
[5] *GSI Helmholtz Center for Heavy Ion Research, Planckstrasse 1, 64291 Darmstadt, Germany*
[6] *John-von-Neumann Institute for Computing (NIC), FZ Jülich, 52425 Jülich, Germany*

(Received 15 December 2020; accepted 14 May 2021; published 1 June 2021)

Central nucleus-nucleus collisions produce many new baryons and the nuclear clusters can be formed from these species. The phenomenological coalescence models were used extensively for description of light nuclei from these baryons in a very broad range of collision energies. We suggest that the coalescence nucleation process can be effectively considered as (1) the formation of low-density baryon matter which can be subdivided into primary diluted clusters with the limited excitation energy, and (2) the following statistical decay of such clusters leading to the final cold nuclei production. We argue that the nuclei formation from the interacting baryons is a natural consequence of the nuclear interaction at subnuclear densities resulting in the nuclear liquid-gas-type phase transition in finite systems. In this way one can provide a consistent interpretation of the experimental fragment yields (FOPI data), including the important collision energy dependence of He isotope production in relativistic ion reactions. We investigate the regularities of this new kind of fragment production, for example, their yield, isospin, and kinetic energy characteristics. A generalization of such a clusterization mechanism for hypernuclear matter is suggested. The isotope yields and particle correlations should be adequate for studying these phenomena.

DOI: 10.1103/PhysRevC.103.064602

I. INTRODUCTION

The production of nuclear fragments in relativistic nuclear reactions is one of the important topics in nuclear physics. It is known since the late 1970s that many different light complex nuclei can be produced in central nucleus-nucleus collisions [1]. Usually it is associated with a coalescence-like mechanism, i.e., the complex particle are formed from the dynamically produced nucleons and other baryons, because of their attractive interaction. The coalescence model has demonstrated a good description of the data (by adjusting the coalescence parameter) from intermediate to very high collision energies [2–4]. There were many other intensive investigations of the coalescence mechanism, e.g., see the latest Refs. [5–7]. This supports the idea that the baryons emerging after the initial dynamical stage are the main constituents of these nuclei.

As we know also, many nuclear fragments can be produced in peripheral collisions as a result of multifragmentation of hot projectile/targetlike residual nuclei. A lot of experiments was devoted to this study associated with the nuclear liquid-gas type phase transition. In particular, ALADIN [8–11], EOS [12], ISIS [13,14], FASA [15], and other experimental collaborations have provided very high quality data. From the theoretical side, many dynamical and statistical models were developed. Here we recall the success of the hybrid approaches, which include the descriptions of the nonequilibrium dynamical reaction stage and the following decay of the equilibrated nuclear sources. The description of the last stage with the statistical models was very instructive (see, e.g., SMM [16] and MMMC [17]). These statistical models provide the generalization of the liquid-gas type phase transition phenomenon to finite nuclear systems. The success of the statistical models in description of the fragment production has encourage to generalize them for hypernuclear matter, and, finally, for production of hypernuclei [18]. The involvement of hyperons (Λ, Σ, Ξ, Ω) obtained in high-energy reactions provides a complementary method to improve traditional nuclear studies and opens new horizons for studying particle physics and nuclear astrophysics (see, e.g., Refs. [19–23] and references therein). Previously we have theoretically investigated the production regularities of large hypernuclei which can originate from peripheral nucleus-nucleus collisions. In this case the produced strange particles are captured by the projectile and target residues. In particular, we have demonstrated a big yield of such hypernuclei, their broad distribution in mass and isospin, and a considerable production of multistrange hypernuclei [24–27]. This opens new possibilities for their investigation in comparison with traditional hypernuclei experiments with light particles.

However, many modern experimental detectors for heavy-ion collisions are designed to measure particles produced in midrapidity reaction zone. Presently, some experimental collaborations (STAR at RHIC [28], ALICE at LHC [29], CBM [30], BM@N, MPD at NICA [31]) plan to investigate light nuclei clusters and their properties in reactions induced by relativistic hadrons and ions. Therefore, in this paper we concentrate on the production of light nuclei (and hypernuclei) coming from central high-energy collisions.

To understand these nuclei formation process we apply theoretical methods, which were partly developed earlier, e.g., for the coalescence procedure [32]. In this paper we emphasize another aspect of this phenomenon: The coalescent clusters can be sufficiently large and present pieces of nuclear matter at subnuclear densities. They can have some excitation energy and their following evolution can be described by the statistical methods. Moreover, the decay of these excited clusters can be treated by basing on the previous theoretical and experimental achievements concerning nuclear multifragmentation phenomena. Contrary to the standard coalescence picture which considers only baryons combining into a final nucleus the new picture includes effectively many body interaction, also with baryons which were not captured in the final nuclei. This novel development leads to the qualitatively new predictions and can explain experimental data which were never analyzed before. Below we demonstrate the important new findings and compare our results with recent FOPI experimental data [33,34].

II. PHYSICAL MEANING OF THE COALESCENCE INTO HOT CLUSTERS

The normal and strange baryons are abundantly produced in high-energy particle reactions, e.g., nucleus-nucleus, hadron-nucleus and lepton-nucleus collisions. For description of this process one can use the transport models, like UrQMD [35,36], HSD [37], IQMD [38], GiBUU [39], and others. These models generate baryons coming from primary and secondary particle interactions, including the rescattering and decay of resonances. In the end of the dynamical stage these produced baryons can also attract each other and form clusters. The phenomenological coalescence models are usually adjusted to describe the cluster yield by using a coalescence parameter. The success in description of the experimental data (see, e.g., Refs. [2–7] and references in) tells us that the clusters can really be consisted of the dynamical baryons. However, it does not tell us about the phase space distribution of the involved baryons, and on properties of the formed clusters. As a rule, the transport models designed to describe high-energy interactions have no possibilities to follow precisely low energy interactions between nucleons leading to the nucleus formation at low densities.

In the end of the dynamical stage (at time around ∼10-30 fm/c after the beginning of the nucleus collision) some produced baryons can be located in the vicinity of each other with local subnuclear densities around $0.1\rho_0$ ($\rho_0 \approx 0.15$ fm^{-3} is the normal nuclear density). The momenta of these baryons are obtained from primary nucleons and other hadrons interactions during their collisions. These particles are mostly concentrated in the midrapidity region. We expect that by this time the fast produced particles, as well as the nucleons of projectile and target residue, have separated sufficiently, so the hard interactions leading to the new particle formation are practically stopped. Such kind a saturation is demonstrated in many transport approaches [24]. For this reason one can also expect that if some baryonic clusters are possibly formed via dynamical correlations in earlier times they will be destroyed by intensive interactions existing at large densities. At the subnuclear density the baryons in the coordinate vicinity will still have an attractive nuclear interaction and may form new baryon clusters. Since the baryons can move respect to each other inside these clusters, we may say we are dealing with the excited clusters. Actually, in our approach we can consider a general situation of baryonic nuclear matter expanding as a result of the previous dynamical process. The new idea is that our coalescence procedure can be presented as a division of the all low-density matter into small parts (clusters) with baryons which are in equilibrium respective to the nucleation process. These clusters are analogous to the local freeze-out states for the liquid-gas type phase coexistence adopted in statistical models. The following evolution of such clusters, including the formation of nuclei from these baryons, can be described in the statistical way. Within our procedure it means that these hot clusters decay into nuclei. It is interesting that this statistical decay of finite systems leads to a universal scaling behavior of the nuclei yields with the system size, as known from the multifragmentation studies also. We emphasize a very important difference of our mechanism from the standard coalescence: It is assumed in the simplistic coalescence picture that only baryons which combine a bound nucleus can interact in the final state. All other baryons will not interact with this nucleus, or interact very slightly by taking extra energy to conserve the momentum/energy balance. In our case, the baryons of the primary hot coalescent cluster may be unbound but they interact intensively to produce final nuclei. As a result not all these baryons will be bound in the nuclei in the end.

Here the crucial point is if the lifetime of these clusters is sufficient for equilibration between the baryons to be considered as statistical systems and to apply the statistical methods. We remind that the lifetime of finite nuclear species is related to the energy accumulated into these species. We know from the extensive studies of nuclear multifragmentation reactions [9–11,16,17] that the excitation energies of the excited nuclear systems can reach up to 8–10 MeV per nucleon, and the statistical models describe their disintegration very good. We have also learned from the analysis of nuclei production in multifragmentation that the densities before the break-up of these systems are around 0.1-$0.3\rho_0$, and their lifetime is 50–100 fm/c [13,15]. We believe that the difference between the multifragmentation of excited projectile- and targetlike sources and formation of the baryon clusters in central collisions is just in the dynamical mechanisms leading to these diluted finite systems. In the standard multifragmentation the systems are prepared via dynamical knocked many nucleons and thermal (or dynamical) expansion of the remaining nuclei. Our cluster systems are prepared just as a result of the local interaction (e.g., attraction) of the stochastically produced primary baryons. Therefore, we can suggest that the energy around ∼10 MeV per nucleon could be a reasonable value which can be reached in such hot coalescent clusters, similar to the standard multifragmentation case. If the excitation energy is much higher, then the existence of such clusters as intermediate finite systems with their following evolution in the statistical way become problematic. However, the final conclusion on the excitation energy should be done after the detail comparison with experiment.

III. SIMULATIONS OF PRODUCED BARYONS AND THEIR COALESCENCE

It is natural to use the transport models for the generation of baryon parameters (coordinates and momenta) after their dynamical production in relativistic nucleus collisions. As an approximation we can employ the Dubna cascade model (DCM) which has demonstrated a good performance in description of many experimental data [2,24,27]. According to the construction this model provides a defined time-end of the fast reaction stage and gives the corresponding parameters of baryons. In the following we note it as G1 generation. However, to understand the coalescence and following de-excitation processes better, as an initial step we'll use the distributions of baryons in kinetic energy obtained within other models which have clear physical interpretation. It is instructive to consider a simple expanded nuclear matter with stochastically distributed baryons. Our second method is noted as G2 generation: We perform the isotropic generation of all baryons of the excited sources according the microcanonical momentum phase space distribution with the total momentum and energy conservation. It is assumed that all particles are in a large freeze-out volume (at subnuclear densities) where they can still interact to populate uniformly the phase space. Technically, it is done with the Monte Carlo method applied previously in the SMM and Fermi-break-up model in the microcanonical way [16], and taking into account the relativistic effects according to the relativistic connection between momentum $\vec{p}$, mass m, and kinetic energy of particles E_0, see Eq. (1) (where the sum is over all particles and all ingredients are taken in the energy units):

$$\sum \sqrt{\vec{p}^2 + m^2} = E_0 + \sum m. \tag{1}$$

The total energy available for kinetic motion of baryons E_0 (we call it as the source energy) is the important parameter which can be adjusted to describe the energy introduced into the system after the dynamical stage. We believe G2 generation can be considered as one of the reasonable cases since there are very intensive interactions between colliding nucleons of target and projectile, which take place in some extended volume during the reaction and may lead to the equilibration in the one-particle degrees of freedom. In this case we do not take directly into account the coordinates of the baryons but we assume they are proportional to their velocities and strictly correlate with them.

In the third method, G3 generator, we assume the momentum generation similar to the explosive hydrodynamical process when all nucleons fly out from the center of the system with the velocities exactly proportional to their coordinate distance to the center of mass. For this purpose, with the Monte Carlo method, we place uniformly all nucleons inside the sphere with the radius $FR_nA_0^{1/3}$ without overlapping. Here A_0 is the nucleon number, and $R_n \approx 1.2$ fm is the nucleon radius. The size factor $F \approx 3$ is assumed for the expanded freeze-out volume in which the nucleon can still strongly interact with each other. At the intermediate collision energies this volume corresponds approximately to the average expansion of the system after simulations with the transport models, when the baryon interaction rate drastically decreases. Finally, we attribute to each nucleon the velocity by taking into account the momentum and energy conservation for the relativistic case [Eq. (1)]. Obviously, the velocities and coordinates of baryons are strongly correlated with each other. It is obvious that both G2 and G3 generators suggest the baryonic matter expanded in each coordinate point. All parts of this matter do certainly pass the "freeze-out" density where nuclei can be still formed. We think it is important to consider these cases for our study.

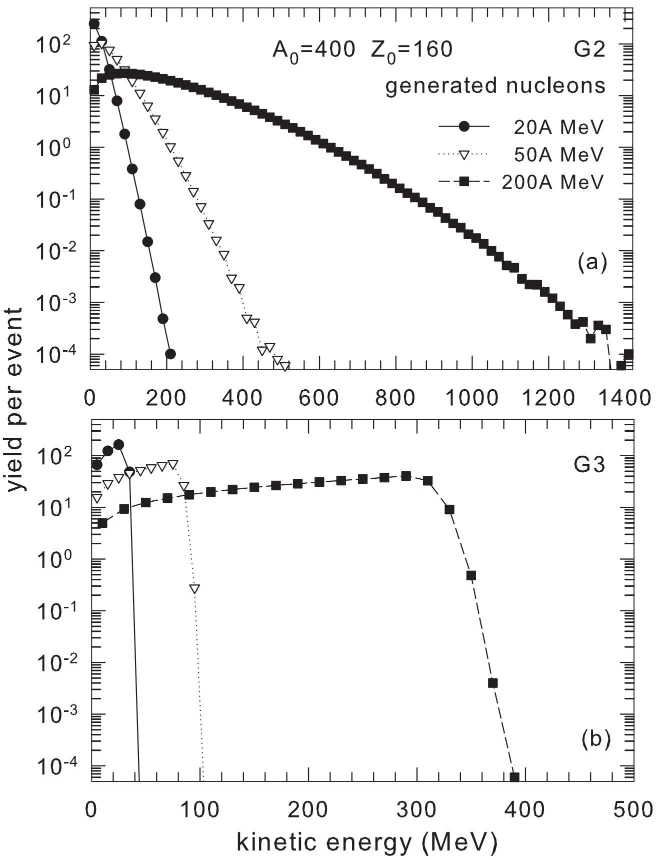

FIG. 1. Energy spectra for initial nucleons of the hot expanding nuclear system according to the microcanonical phase space distribution—G2 (a), and according to the hydrodynamicallike explosion—G3 (b). The suggested total kinetic energies are 20*A* MeV, 50*A* MeV, and 200*A* MeV. The nucleon source size and composition are shown in panel (a).

In the Fig. 1(a) we demonstrate the energy distribution of all initial nucleons in the excited source with mass number $A_0 = 400$, charge $Z_0 = 160$, after G2 generation. The source energy (i.e., the total kinetic energies of all nucleons) were taken as $E_0 = 20A$ MeV, $50A$ MeV, and $200A$ MeV. This may characterize the hot systems produced at central collisions of heavy nuclei at laboratory energies around $100A$-$1000A$ MeV. As expected, the distributions are very broad. We have also checked that the size effect on the distributions is practically minimal, as it is following thermodynamical quantities in the one-particle approximation. In the Fig. 1(b) we show the same distributions but for G3 generation. It is seen a qualitative difference of the nucleon energy distributions after G2 and G3 generators. G3 provides a very compact distribution of nucleons according to their positions in the freeze-out volume. We think it is important to demonstrate how this difference will be manifested in the cluster production and the kinetic energy of clusters.

As discussed, because the baryons produced at the dynamical stage can fluctuate in the momentum space, and this can also be correlated with their locations in the coordinate space, we can divide the matter into the primary baryon clusters (i.e., the primary clusters appear due to geometric phase-space correlations). The subtle interactions (attraction) inside these primary clusters can lead to the final nuclei formation. To describe the subdivision into such clusters we use the coalescence prescription, and apply the coalescence of baryon (CB) model [32,40]. In G2 and G3 cases the criterion is the proximity of the velocities (or momenta) of nucleons. As was mentioned, in these cases we do not include explicitly the coordinate of nucleons, since this kind of generation suggests a correlation of velocities and space coordinates. In particular, the coordinate vectors should be directly proportional to the velocities vectors. So the velocity coalescence parameter is sufficient for the cluster identification in these models. Such a correlation exists in many explosive processes and it influences the original clusterization. However, for the following evaluation of the cluster properties we assume that such clusters with nucleons inside have the density of $\rho_c \approx \frac{1}{6}\rho_0$ as it was established in the previous studies of statistical multifragmentation process [13,15–17]. This corresponds to the average distance of around 2 fm between neighbor nucleons, and these nucleons can still interact leading to the nuclei formation. It is also consistent with the densities which can be obtained for such clusters with the transport model calculations in the end of the dynamical stage (see Sec. V). Within the CB model we suggest that baryons (both nucleons and hyperons) can produce a cluster with mass number A if their velocities relative to the center-of-mass velocity of the cluster is less than v_c. Accordingly, we require $|\vec{v}_i - \vec{v}_{\rm cm}| < v_c$ for all $i = 1, ..., A$, where $\vec{v}_{\rm cm} = \frac{1}{E_A}\sum_{i=1}^{A}\vec{p}_i$ ($\vec{p}_i$ are momenta and E_A is the sum energy of the baryons in the cluster). This is performed by sequential comparison of the velocities of all baryons. As done before [32,40], to avoid the problem related to the sequence of nucleons within the algorithm, we apply the iterative coalescence procedure, starting from the diminished coalescence parameters for clusters and by increasing them step-by-step up to the v_c value.

We show in Fig. 2 the distributions of clusters in their mass number A after the coalescence of initial nucleons of the primary source $A_0 = 100$, $Z_0 = 40$ (a), and $A_0 = 400$, $Z_0 = 160$ [(b) and (c)], for $E_0 = 50A$ MeV, for the velocity coalescence parameter $v_c = 0.07$, 0.14, and 0.22 c. In our case, v_c means the maximum velocity deviation and all baryons with lower relative velocities do compose a cluster. The largest $v_c = 0.22$ c is approximately of the order of the Fermi-velocity which is expected in such nuclei. The smallest $v_c = 0.07$ c is consistent with the coalescence parameters extracted previously in analyses of experimental data [2,3]. In the latest case the cluster excitation energy is minimal and the cluster may not decay by the nucleon emission.

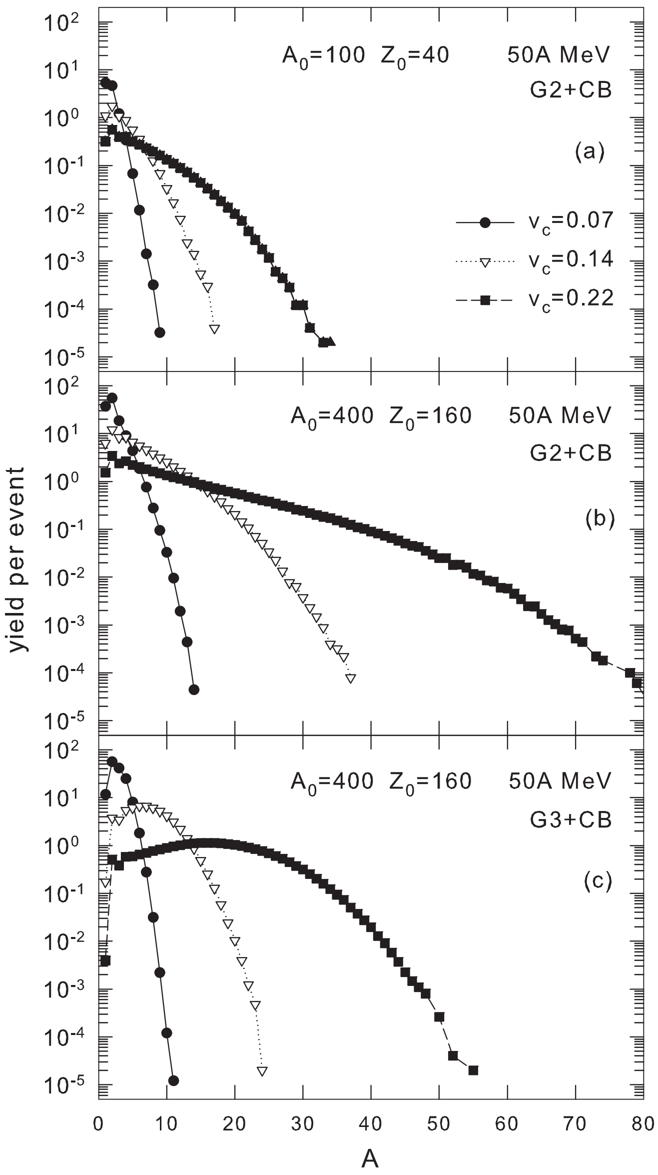

FIG. 2. Yield of coalescent clusters versus their mass number A after the CB calculations at the source energy of $50A$ MeV. Composition and sizes of sources, nucleon generators (G2 and G3), as well as coalescence parameters (v_c) are indicated in panels (a), (b), and (c).

One can see that the big clusters indeed can be produced with the coalescence mechanism. It was discussed previously [32,40], however, without determining the cluster properties. By comparing Figs. 2(a) and 2(b) it is instructive to note

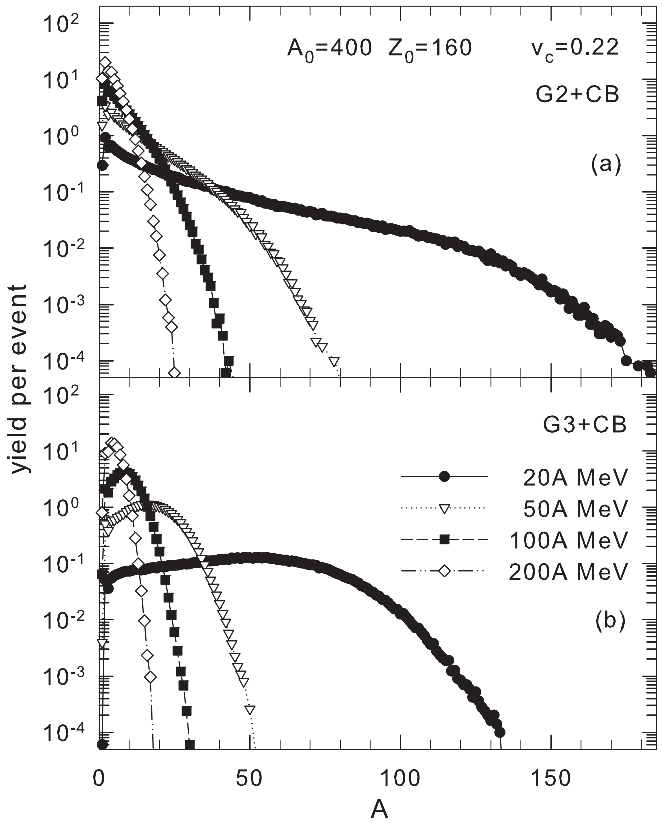

FIG. 3. The same as in Fig. 2 but for fixed coalescence parameter $v_c = 0.22\ c$, G2 and G3 generators. The source composition and energies are shown in panels (a) and (b).

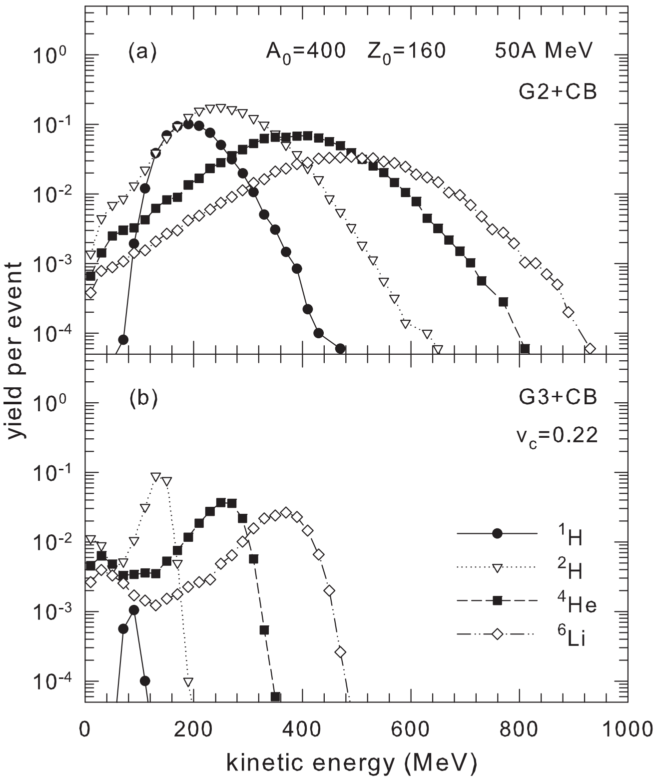

FIG. 4. Energy distributions of protons and some light particles after the coalescence. The source characteristics, baryon generators, coalescence parameter, and produced species are indicated in panels (a) and (b).

that the bigger source can produce larger clusters at the same initial excitation per nucleon. This is a typical collective effect coming from the larger number of nucleons involved in the reaction. It is obvious that a larger coalescence parameter leads to the formation of bigger clusters. Still, as will be shown below, their excitation energies will be also higher, and their subsequent decay decreases the nuclei sizes. By comparing the results after G2 and G3 generators [Figs. 2(b) and 2(c)] one can see an essential difference in the produced clusters. In the last case the cluster have large sizes which are likely grouped around the mean values with the maximum yield. This is the consequence of flowlike initial distribution of baryons. However, in G2 case we can get very big clusters, however, with a low probability. They come from the low-energy component of the G2 nucleon energy distribution.

It is important to understand how the masses of coalescent clusters evolve with the source energy. In Fig. 3 we demonstrate the mass distributions in the biggest sources at the parameter $v_c = 0.22\ c$ for the wide range of E_0. The yields of big clusters are larger at the low source energy, since the velocities of nucleons are smaller and closer to each other to form a cluster. However, there are a lot of intermediate mass clusters (with $A \gtrsim 10$) even at high source energies. It is a consequence of the stochastic nature for production of such nucleons since they may appear in the phase space vicinity of other nucleons. Under the assumptions of G2 and G3 generators we simulate it by the Monte Carlo method. The considered source energies correspond to nucleons originated from central heavy ion collisions with beam energies less than 1 A GeV.

The kinetic energy of produced clusters is also an important characteristic which can give experimental evidences about baryons composing clusters. Figure 4 demonstrates the kinetic energies of the remaining protons, and clusters ^{2}H, ^{4}He, and ^{6}Li after the coalescence in the $A_0 = 400$, $Z_0 = 160$, $E_0 = 50A$ MeV source, for $v_c = 0.22\ c$. It is clearly seen that, for example, the spectrum for remaining protons is essentially different from the initial distributions of nucleons shown in Fig. 1: The reason is that a lot of protons are captured by primary clusters. In G3 case practically all protons are in coalescent clusters. After decay of the excited clusters many protons may become free again (see Fig. 10), however, this additional interaction via the clusterization may change their energy spectra. One can see also that the energy distributions of the produced clusters have a flowlike structure, i.e., each captured nucleon adds the kinetic energy to the cluster. It is especially seen in G3 case, where the kinetic energy of clusters with the maximum yield is nearly directly proportional to their mass number.

In addition, these clusters can have very exotic isospin composition. This is a direct consequence of the initial random distribution of protons and neutrons in the phase space. In Fig. 5 we demonstrate such broad isotope distributions for few elements. It is clear from general properties of nuclei that

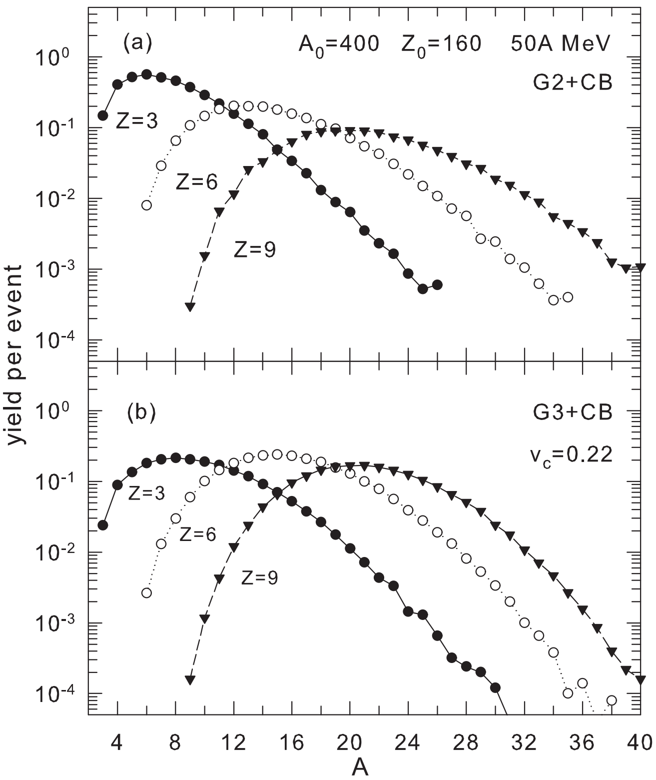

FIG. 5. Isotope distributions of elements with charges $Z = 3$, 6 and 9 after the coalescence in the sources after G2 (a) and G3 (b) baryon generators. The source sizes, energies and coalescence parameter are shown in panels (a) and (b).

these isotopes can not be stable and must decay afterwards. However, this decay will take place during the time which is more prolonged than the dynamical reaction stage. As a result of the secondary processes we can expect very exotic nuclear species in these reactions. We have found also that the bigger source can be responsible for larger neutron enrichment and, consequently, more exotic nuclei.

As well known the nuclei have many excited states which decay during the time much longer than the dynamical (collision) reaction time which is around few tens fm/c. Generally, we expect that during the coalescence process the highly excited coalescence clusters can be produced. Within our approach, as we have discussed in Sec. II, the subtle interaction of dynamically produced baryons can result into excited systems which decay later on in a statistical way. The energy accumulated in such low-density finite systems is the main ingredient which determines their following evolution. It can be evaluated in various approximations. In the lowest limit we can estimate this excitation as a relative motion of the nucleons initially captured into a cluster respective to the center of mass of this cluster. In this case the excitation energy E^* of the clusters with mass number A and charge Z is calculated as

$$E^* = \sum_{i=1}^{A} \sqrt{\vec{p}_{ri}^{\,2} + m_i^2} - M_A, \tag{2}$$

where M_A is the sum mass of nucleons in this nuclear cluster, $i = 1, ..., A$ enumerate nucleons in the cluster, m_i are the masses of the individual nucleons in the cluster, $\vec{p}_{ri}$ are their relative momenta (respective to the center mass of the cluster). However, in the cluster volume the nucleons can interact with each other and the binding interaction energy δE^* should be added to the E^*. As an upper limit we can take the ground-state binding energy of normal nuclei with A and Z. However, since our clusters present pieces of nuclear matter expanded already during the previous dynamical reaction stage, we believe that in fact this energy should be lower. Therefore, as the first approximation we use the following recipe for evaluation of δE^*: It is known the ground-state binding energy of nuclei can be written as the sum of short range contributions (E_{sr}, which naturally includes volume, symmetry, surface energies), and the long-range Coulomb energy (E_{col}), see, e.g., Ref. [16]. Since a cluster is extended its Coulomb energy contribution will be smaller and we can recalculate it proportional to $(\frac{\rho_c}{\rho_0})^{1/3}$ (in the Wigner-Seitz approximation [16]). For the short range energies, it is assumed that all contributions do also decreases proportional to $(\frac{\rho_c}{\rho_0})^{2/3}$ as it follows from the decreasing of the Fermi energy of nuclear systems. In future the problem of the energy deposited into the dilute unbound systems after the dynamical stage should be investigated in

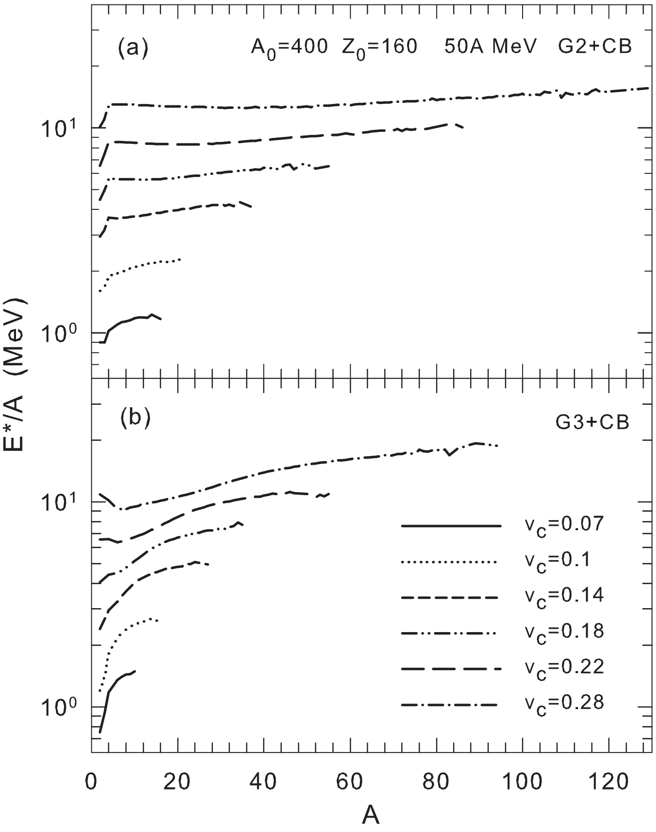

FIG. 6. Average internal energy of coalescent clusters versus their mass number A produced as a result of the coalescence (CB) in the sources with $A_0 = 400$ and $Z_0 = 160$ after G2 (a) and G3 (b). The source energy and coalescence parameters are shown in panels (a) and (b).

details. In this first work we use

$$\delta E^* = E_{\rm col}\left(\frac{\rho_c}{\rho_0}\right)^{1/3} + E_{\rm sr}\left(\frac{\rho_c}{\rho_0}\right)^{2/3}, \qquad (3)$$

since it provides a reasonable estimate in between the two limits. In the following we call this energy as the cluster excitation energy, or the cluster internal energy, which is defined above the individual baryon masses. Further we take it for the statistical calculations of the nucleation process (e.g., the cluster decay) which naturally include the ground-state masses of produced nuclei.

As usual we consider the cases of both G2 and G3 baryon generators. In Fig. 6 we present the average internal energies of such clusters versus their mass number for the big systems $A_0 = 400$, $Z_0 = 160$, and $E_0 = 50A$ MeV, with the coalescence parameters v_c from 0.07, to 0.28 c. One can see that the internal energy per nucleon increases with this parameter. This is because more nucleons with large relative velocities are captured into the same cluster. By comparing the panels of Fig. 6 we see the effect of the source generator on these distributions: The internal energies are not very different, since they are determined by relative nucleon motions inside clusters. Nevertheless the G3 provides a general increase of the internal energy with the mass number since the large clusters are consisting of baryons having initially higher velocities.

IV. DISINTEGRATION OF HOT COALESCENT CLUSTERS

It is clear that our primary coalescent nuclear clusters must disintegrate into small peaces because of their big internal excitation energy. As we discussed in Sec. II the whole process of both the formation and subsequent decay of such clusters is the necessary part of one physical phenomenon. It can be considered as a result of the residual nuclear interaction between baryons at the subnuclear density leading to the production of final nuclear species. In the end the cold and stable nuclei are produced. At this point it is instructive to recall the previous analyses of experimental data on disintegration of excited nuclear systems [8–17]. This investigation has lead to the conclusions on the statistical nature of such disintegration. Also it was discussed that this process can be the manifestation of the liquid-gas type phase transition in finite nuclei systems [16]. We remind, it was obtained in these theoretical analyses [9–11,17] that there is the limitation for the excitation energy for the finite thermalized nuclear systems, around 10 MeV per nucleon, with values closed to the binding energies of the systems. As was established these systems decay in time about ~100 fm/c [13–15] that is several times longer than the dynamical reaction stage. This result is obtained in multifragmentation of nuclear residues produced in peripheral relativistic ion collisions. We believe that it is a general property of finite nuclear systems: Independent on the way how the primary excited clusters are formed, they can be considered as small systems of interacting nucleons in the region of the nuclear-liquid gas coexistence. As a result we can also expect the same limitation in the excitation energy of our coalescent clusters. This puts natural limits on the values of the parameters v_c for the coalescence mechanism in central nuclei collisions. In the following we can apply the well established statistical models for the cluster de-excitation.

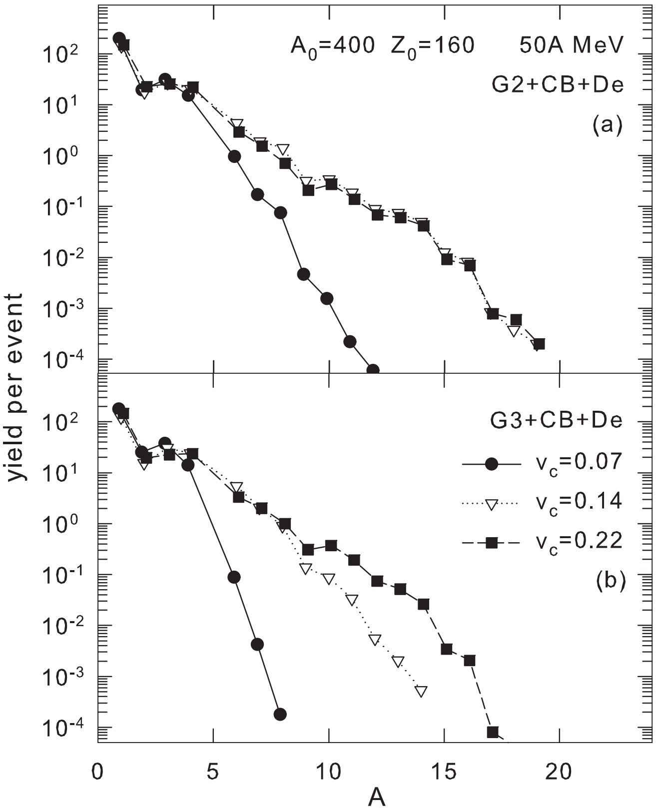

FIG. 7. Yield of final cold fragments versus their mass number A after the coalescence and fragment de-excitation (CB + De) calculations at the source energy of 50A MeV. Baryon generators, composition and sizes of sources, as well as coalescence parameters are shown in panels (a) and (b).

As was done previously in relativistic peripheral collisions and heavy-ion collisions at low energies we involve the statistical multifragmentation model (SMM) [16] to describe the break-up of normal nuclear clusters. This approach includes the consistently connected multifragmentation, evaporation, fission (for large nuclear systems), and Fermi-break-up (for small systems) models. At the same time it reflects general-properties of nuclear matter resulting into the phase transition. The Fermi-break-up model, which reasonably good describes experimental data on disintegration of light nuclei, was generalized also for hypernuclear systems in Ref. [41]. As well as the evaporation and fission models were generalized for hypernuclei [26], and were involved for break-up simulations of heavy clusters. Below we demonstrate the results obtained after the disintegration of hot primary coalescent clusters into the final cold nuclei.

The secondary de-excitation of primary clusters changes dramatically all characteristics of yields and spectra of the nuclei. In Figs. 7 and 8 we demonstrate how the mass distributions of fragments, shown previously in Figs. 2 and 3, will change after the de-excitation. For clarity we present only few energies E_0 and coalescence parameters v_c for the both baryon generators. It is obviously that the fragment sizes decreases

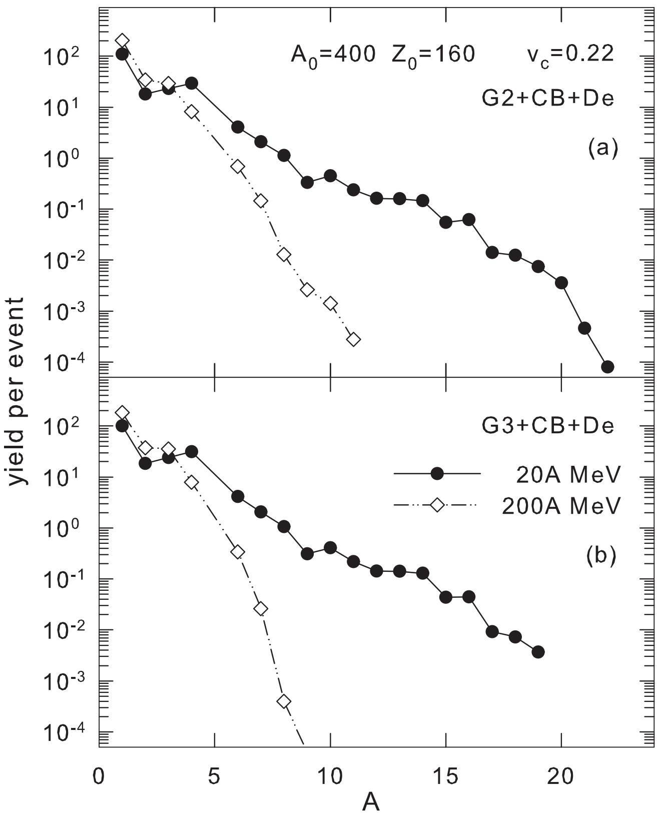

FIG. 8. Yield of final cold fragments versus their mass number A after the coalescence and fragment de-excitation (CB + De) calculations at the source energies of 20*A* MeV and 200*A* MeV. Baryon generators, composition and size of sources, as well as the coalescence parameter are shown in panels (a) and (b).

considerably because of disintegration of large clusters. In addition, the final fragment distributions behave differently than the primary coalescent ones as function of the coalescence parameter. For example, the increase of v_c is not always leading to the larger fragments: Since the excitation is higher then the bigger hot fragments can decay into smaller peaces too.

The isospin content of final fragments (in Fig. 9) changes also in comparison with the primary coalescent clusters (see Fig. 5). The distributions become more narrow and the obtained isotopes concentrate closer to the stability line. It is expected since these nuclei have largest binding energies. Such a behavior is typical after the statistical disintegration, and it was demonstrated in many previous analysis (see, e.g., Ref. [11]).

Figure 10 shows the energy distribution of protons and light fragments produced after the de-excitation. In comparison with Fig. 4 one can see that many protons with low energy again appear in the system, however, as the de-excitation product. By comparing with Fig. 1 we see also that high-energy protons can appear in the system (G3 case) as a result of coalescence and de-exciation processes. The energies of large fragments can be also lower because they are the products of the decay of even larger clusters which in many cases are composed from the low-energy nucleons. Still the flowlike distribution picture with a local maximum remains for G3 generation.

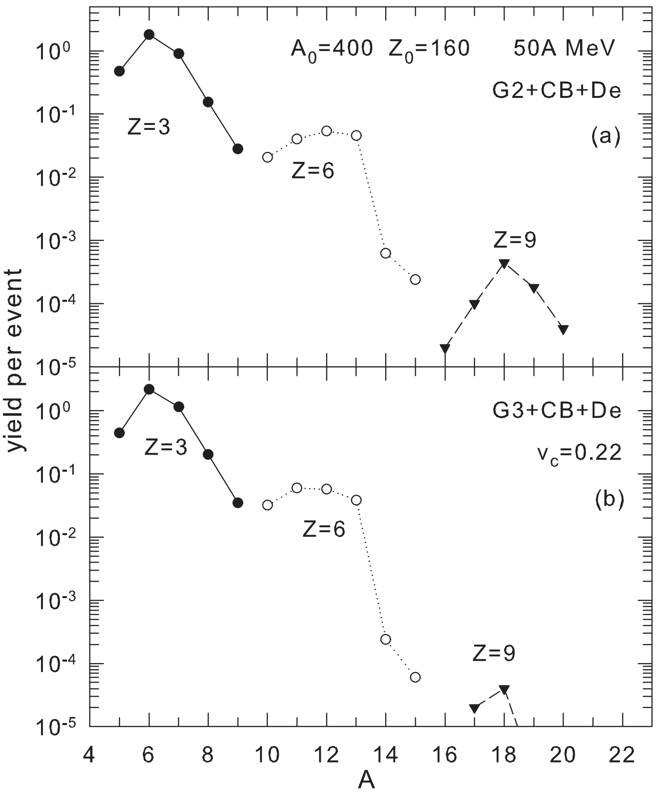

FIG. 9. Isotope distributions of elements with charges $Z = 3$, 6, and 9 after the coalescence (CB) and de-excitation (De). The source composition, energy, and the coalescent parameter are indicated in the figure. The baryon generators G2 (a) and G3 (b) are used.

In Fig. 11 we complement this information with the average kinetic energy per nucleon of these clusters, at different source energies. Figures 11(a) and 11(b) present these energies after G2 and G3 generators respectively. This characteristic can be measured in experiments and it is often associated with a flow energy. We see some important differences in the fragment energies, therefore, it can be used for the identifications of the initial dynamical nucleon distributions. In particular, the kinetic energy per nucleon is slightly decreasing with mass number *A* in the case of the phase space generation G2. This is because the coalescent large fragments are formed predominantly from the slow nucleons which dominate after this generation (see Fig. 1). While after the hydrodynamicallike generation G3 the nucleons with a high energy are enhanced and uniformly distributed in the space. As a result, after the cluster formation and its decay, the fragments from such nucleons have approximately the same flow energy per nucleon: It is evident that the de-excitation leads to smaller fragments, however, their velocities depend on the velocities of the constituent nucleons in the expanded system.

It is instructive to show how the yield of final intermediate mass fragments, for example, with $Z = 3$ can change with the coalescence parameter v_c for various source energies. As we mentioned, there is an interplay of two effects: The increase of

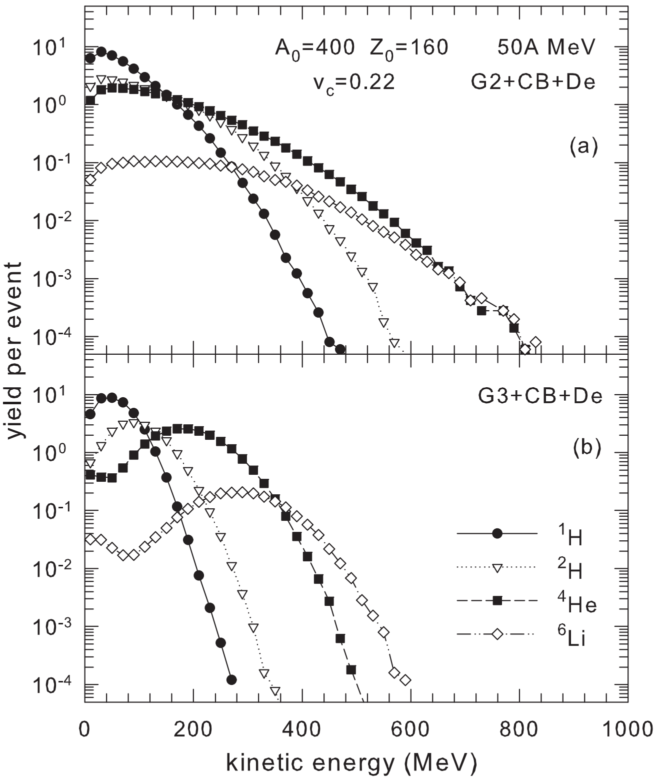

FIG. 10. Energy distributions of protons and some light particles after the coalescence (CB) and the following de-excitation (De). The source composition, coalescence parameter, and produced species are indicated in panels (a) and (b). The baryon generators G2 (a) and G3 (b) are used.

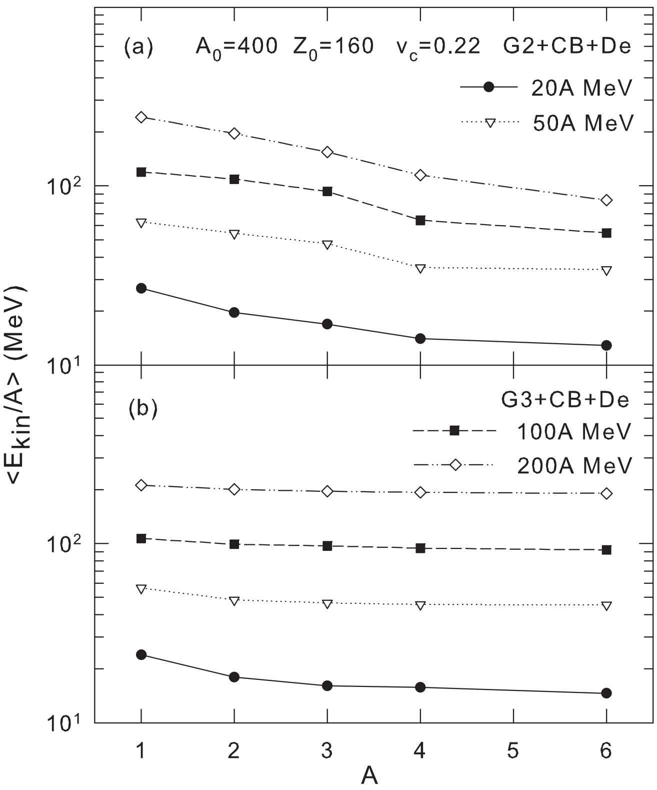

FIG. 11. Average kinetic energies (per nucleon) of fragments versus their mass number A, after the coalescence and the following de-excitation of excited clusters. The generators of initial nucleons G2 (a) and G3 (b) are used. The source composition and energies, coalescence parameter, and produced species are indicated in panels (a) and (b).

v_c leads to large primary coalescent fragments. However, their internal excitation energies are also becoming larger. Therefore, as a result of the de-excitation they break-up into smaller final nuclear species. One can see from Fig. 12 the yield may have a local maximum at some intermediate parameters: There is a trend to increase yields of these fragments with v_c in the region of low v_c and to decrease the yields at high v_c. Also their production decreases for high source energies. This is a quite universal behavior of the fragment production and it is manifested for the both generators.

The production of lightest charged fragments, such as p, ^{2}H, ^{3}H, ^{3}He, and ^{4}He, dominates in central relativistic heavy-ion collisions. Therefore, in Figs. 13 and 14 we show how the corresponding yields depend on the source excitation energy. For clarity we have selected a large v_c which results in big primary clusters with high internal excitation energy (Fig. 13). Also we demonstrate a small v_c corresponding to very low excited coalescent clusters (Fig. 14). We show only the results after G2 generator, since using G3 leads to qualitatively same conclusions.

As expected, the yield difference between protons and complex particles with A=2, 3, 4, and 6 becomes larger at the high source energy, since the system disintegrates into smaller pieces. This is an obvious consequences of a decrease in production of primary coalescent clusters with A. However, at relatively low source excitations, when big primary clusters are still produced, the situation is different. The internal excitation of such clusters is high and the de-excitation results depend on the binding energies of produced species. For this reason the yields of ^{4}He becomes larger than the ^{3}He yields. This result is quite surprising since in the standard coalescence picture (i.e., without de-excitation) the yields of large clusters is always lower than the small ones. And as one see from the both figures this is true for all reasonable coalescence parameters under investigation, though it is more pronounced at large v_c when big primary clusters are abundantly produced. Another interesting result is that the final yield of ^{6}Li can be larger than ^{6}He in the sources, at big v_c. This is also related to the slightly larger binding energy in Li. However, this small effect is lost at small v_c, since the sources are neutron rich and the isospin effect dominates by favoring the formation of neutron rich nuclei. For this reason the comparison of light cluster yields can help to distinguish the internal excitations of primary coalescent clusters and find out the production mechanisms in experiments.

From our experience in multifragmentation reactions, to clarify the fragment production regularities, it is important to look at yields of fragments with $Z \geqslant 3$ too. In Fig. 15 we present the charge yields which can be observed in such experiments. We show again G2 generator calculations since G3 gives qualitatively similar results. As expected for the central

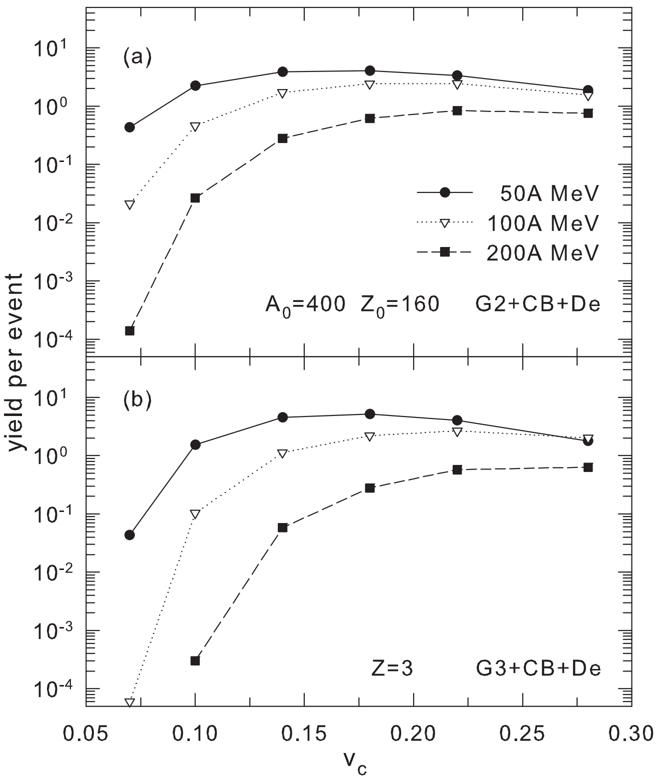

FIG. 12. Yield of $Z = 3$ nuclei as function of the coalescence parameters after the coalescence (CB) and the following de-excitation (De). The nucleon generators G2 (a) and G3 (b) are used. The source composition and their energies are indicated in panels (a) and (b).

collisions of high energy the yield drops with Z nearly exponentially. Obviously, the higher energies lead to the smaller yields of $Z \geqslant 3$. One can conclude from the analysis of this figure, as well as Fig. 12, that yields of big nuclei can be the largest one at intermediate v_c. Since it provides the best balance between the size of primary clusters and their internal excitations leading to the formation of intermediate mass nuclei. Actually, such yields are very sensitive characteristic for the many-body reaction process, and it is complementary to the production of lightest nuclei and protons. Therefore, it should not be disregarded in the analysis of experimental data.

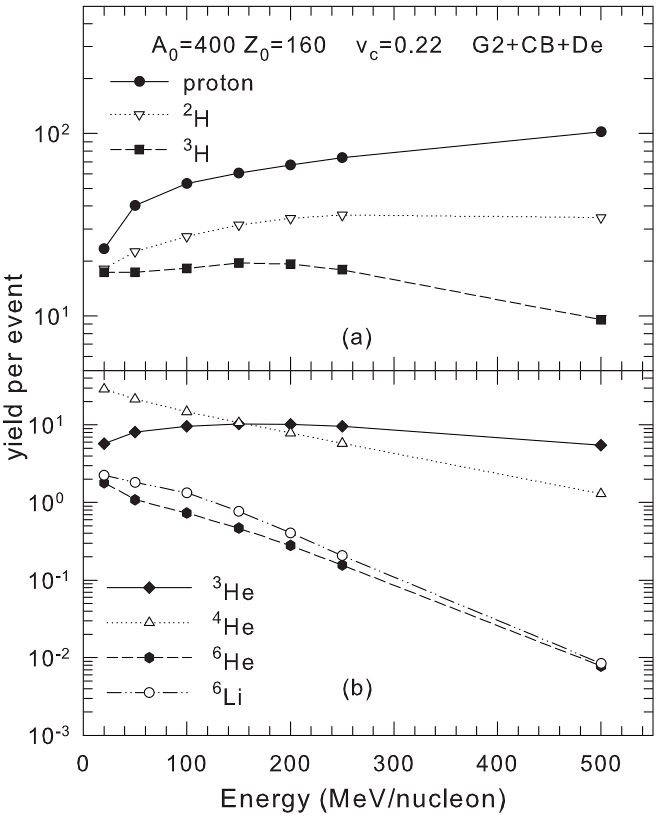

FIG. 13. The yields of protons and light charged particles after G2 generator and the coalescence with de-excitation of hot coalescent clusters (CB + De), as function of the source excitation energy. The coalescence parameter is $v_c = 0.22c$. The notations for the source and particles are shown in panels (a) and (b).

V. TRANSPORT GENERATION OF PARTICLES AND THE STATISTICAL BREAK-UP OF COALESCENT CLUSTERS

Now we consider a practical (and popular) way to treat the relativistic ion collisions with the transport models (see, e.g., Refs. [2,35–39]). These models are able to describe the initial dynamical stage of the collisions with production of many particles including baryons. They are also quite good in description of the experimental data. As the first step we have selected the Dubna cascade model (DCM) which was since long ago on the market and used for analysis of many experiments [2,24,27]. Generally, the transport approach should be more realistic one than the simulation of initial nucleons according to the phase space (G2), and the hydrodynamicallike flow (G3), since it takes into account explicitly the scattering and formation of new baryons. However, if we want to analyze experimental data, then we must take into account the experimental filter and make the same selection of the simulated events as in the experiment. Sometimes it is difficult to do because of the large required statistics. Therefore, the G2 and G3 simulations could be very useful to find the correct way for extracting physical information from the data.

In Fig. 16 we show the proton transverse momenta predicted by the DCM in the case of central (the impact parameter is less than 3 fm) collisions of Au on Au at energies of 250A and 1000A MeV in the laboratory system. For qualitative comparison with our analysis in the previous section we show also the corresponding results obtained with G2 generator for the sources with energies of 50A and 200A MeV for the $A_0 = 400$ and $Z_0 = 160$ system. These source energies are only slightly lower than the corresponding center-of-mass energies of the colliding nuclei. One can see some differences which should influence the following coalescence process. For example, DCM produce more protons with very low transverse momenta and the distributions are more broad.

In the DCM case the same procedure was taken for the coalescence (CB) and de-excitation (SMM) of hot coalescence fragments. However, in the Monte Carlo DCM code the primary nucleons and hyperons can be produced in different time moments during the whole cascade stage which lasts for

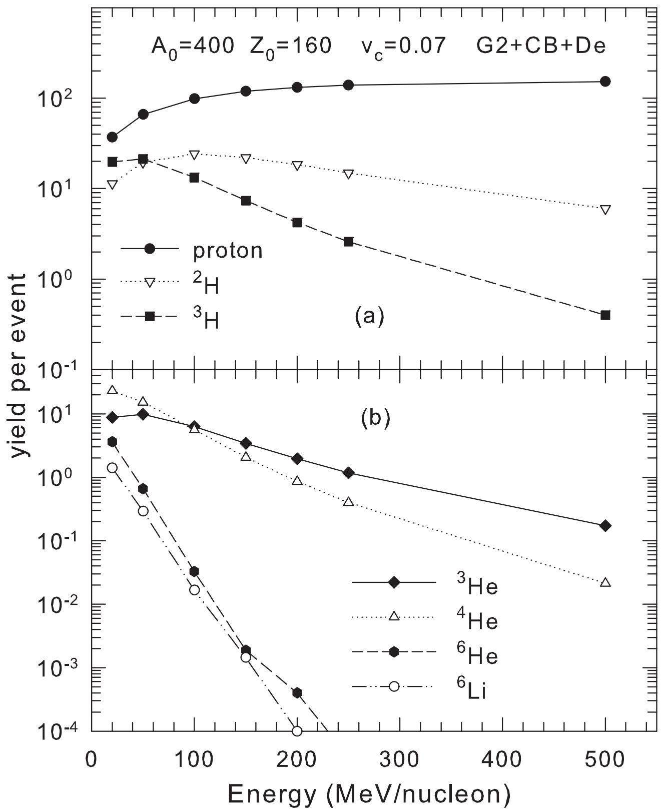

FIG. 14. The same as in Fig. 13 but for the coalescence parameter $v_c = 0.07c$.

10–30 fm/c. Therefore, in addition to the relative velocity coalescence criterion we suggest that the baryons should be close in the coordinate space when this dynamical cascade stage ends. In particular, all baryons consisting of a cluster with mass number A should be inside the sphere with radius of $R = R_0A^{1/3}$ from the center of mass of the cluster. We take $R_0 = 2$ fm, as it is obtained by extracting the freeze-out volume information in the multifragmentation experiments (see Refs. [13–15]), and approximately corresponds to ρ_c density suggested for G2 and G3 generations (see Sec. III).

We present in Fig. 17 the mass distributions of nuclear clusters produced after the coalescence of the cascade nucleons (DCM + CB) and after their following de-excitation (DCM + CB + De) into cold nuclei. As previously we use the SMM model for the de-excitation description. The regularities are similar to the ones demonstrated previously for the excited sources in Figs. 2, 3, 7, and 8. We expect that the quite big nuclei will be observed in experiments at the collision energies around 250A MeV, and there is an essential decrease of their yields with increasing energy up to 1A GeV and to higher energies.

For the same reaction the transverse momentum distributions for ^{2}H and ^{4}He nuclei after both the coalescence and the cluster de-excitation are shown in Fig. 18. The de-excitation leads to the essential production of these nuclei with lower momenta, and to a more steep decrease of spectra with p_t. This trend is more pronounced for large nuclei, therefore, such nuclei should predominantly have low transverse momenta.

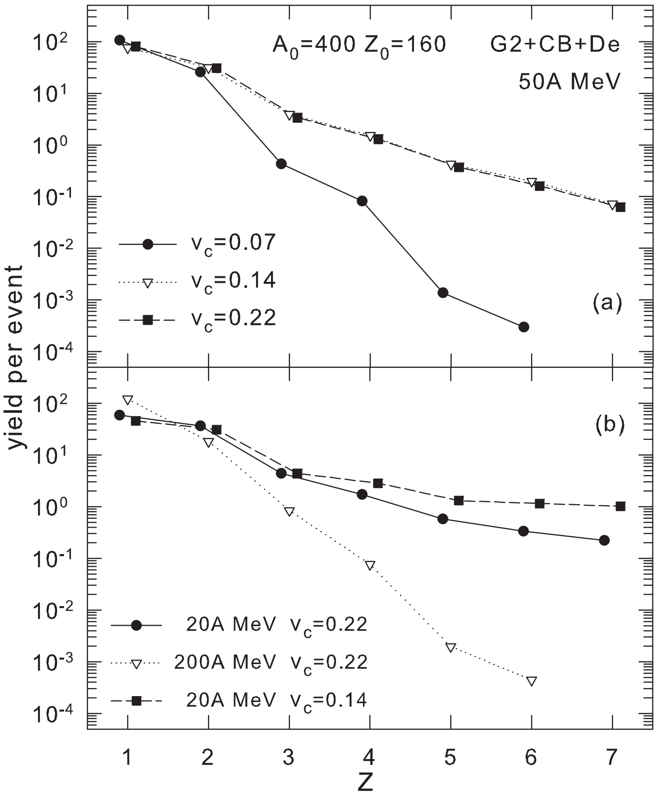

FIG. 15. Charge yields of light and intermediate mass nuclei after the coalescence and de-excitation. The nucleon generator, source composition and energies, and coalescence parameters are indicated in panels (a) and (b).

By using the full DCM + CB + De approach we demonstrate in Fig. 19 how the charge distributions of the final nuclei modify depending on the coalescence parameter v_c and the beam energy. As one can see we have qualitatively the same evolution as was shown in Fig. 15. However, the different initial nucleon distributions lead to slightly different results: In the DCM case of the 250A MeV beam energy the yield of intermediate mass fragments changes very weak with the coalescence parameter. The vicinity of the generated nucleons in the velocity and coordinate space after DCM gives a chance to produce relatively big primary coalescence clusters even at small v_c. In the same time the low excitation energy allows for surviving big fragments after de-excitation. At large v_c the considerably larger clusters are produced. However, they are more excited and can decay into small fragments approximately of the same size as at the smaller v_c. By increasing beam energies this effect disappears and we obtain an expected regular decrease of the charge yields.

The DCM can simulate the production of new baryons, e.g., hyperons. Previously a good comparison of DCM with the strangeness production was shown in Refs. [24,27]. Therefore, the predictions for hypernuclei can be given within same coalescence and statistical de-excitation mechanisms. The coalescence and statistical models were generalized for hyperfragments in Refs. [18,22,26,32,41]. By using this approach we shown the yields of light hypernuclei in Fig. 20.

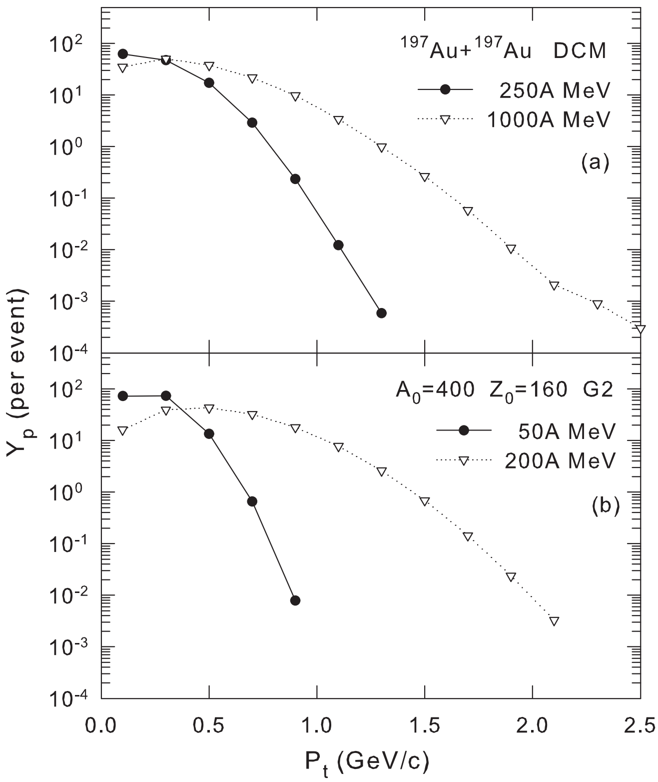

FIG. 16. Transverse momenta distributions of protons produced after the dynamical DCM stage in Au + Au central collisions at energies of 1000*A* MeV and 250*A* MeV (a), and after the phase space disintegration of sources (G2) with energies of 200*A* MeV and 50*A* MeV (b).

We demonstrate some results for the central collisions at the beam energies of 600*A* MeV and 1*A* GeV which are below the threshold for the hyperon formation in nucleon-nucleon interaction. At these energies the Λ hyperons are produced because of the secondary interactions at the cascade stage. Actually, the hypernuclei from such subthreshold processes are very important since their productions depends on subtle details of hyperon-nucleon interactions. Besides well known hydrogen and helium hypernuclei in Fig. 20(a) we show predictions for exotic neutron-Λ (NΛ), proton-Λ (^{2}H$_\Lambda$), and neutron-neutron-Λ (NNΛ) hypernuclei, which are discussed in the literature [29,42] to facilitate their experimental searching.

We believe it would be instructive to justify in experiment directly the secondary de-excitation of primary coalescent hyperclusters. For this purpose in Fig. 20(b) we demonstrate the decay channels leading to the production of $^3_\Lambda$H nuclei for the 1*A* GeV energy case. The charged particles can be easily detected in modern experiments and this correlation measurement would be important confirmation of the reaction mechanism.

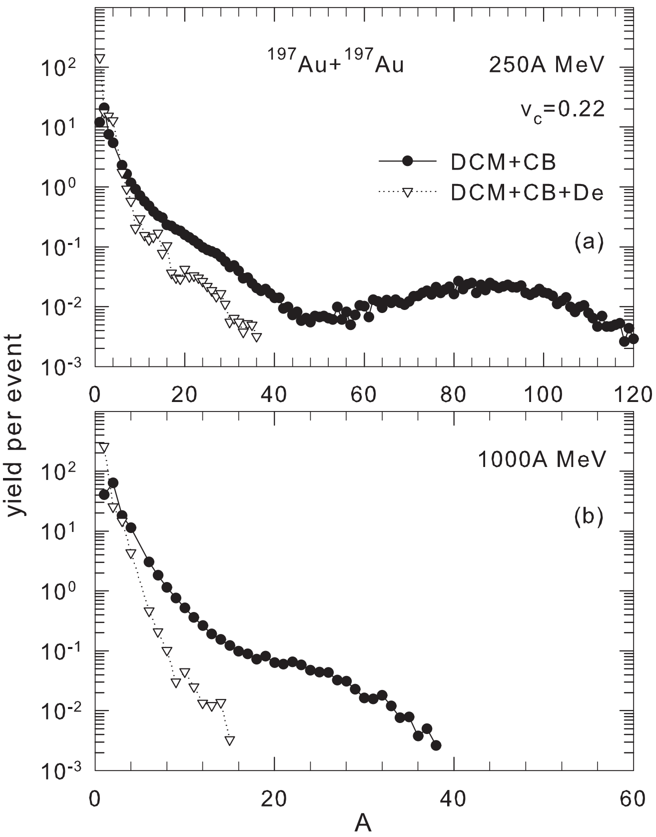

FIG. 17. Calculated distributions of coalescent clusters (after DCM and coalescence: DCM + CB) and final nuclei (after de-excitation: DCM + CB + De) in mass number. Beam energies of central collisions of gold nuclei and the coalescence parameter are shown in panels (a) and (b).

VI. ANALYSIS OF FOPI EXPERIMENTAL DATA

To confirm the proposed mechanisms we should analyze experimental data. We have selected the FOPI data on light nuclei produced in central Au + Au collisions, since they are the most full and systematic ones in the present time [34]. There were attempts to analyze it with the coalescence and statistical prescriptions [4,6]. We should note that these data are obtained with the selection of the central collisions with the ERAT criterion [33], which suggests a considerable isotropy of the produced particles in the center of mass system. This isotropy is naturally provided by the G2 and G3 generations. We have found from the momentum analysis that the DCM calculations are not able to provide such an isotropy for central events. Because DCM predicts much more nucleons with low transverse momenta (see, for example, the comparison presented in Fig. 16). In principle, the DCM sample can be improved by drastic increasing the statistics and by the special selecting the central events which fulfill the ERAT criterion. That would require much more Monte Carlo simulations. However, the goal of our present analysis is to show the consistency of our approach to the observations. We believe that the simple assumptions existing in G2 and G3 generations are sufficient for it. Since they correspond to ones of the possible presentation of the baryon system after multiple rescatterings, and they fulfill all conservation laws and isotropy requirements. In this case we can separate the trends in reproducing the data which

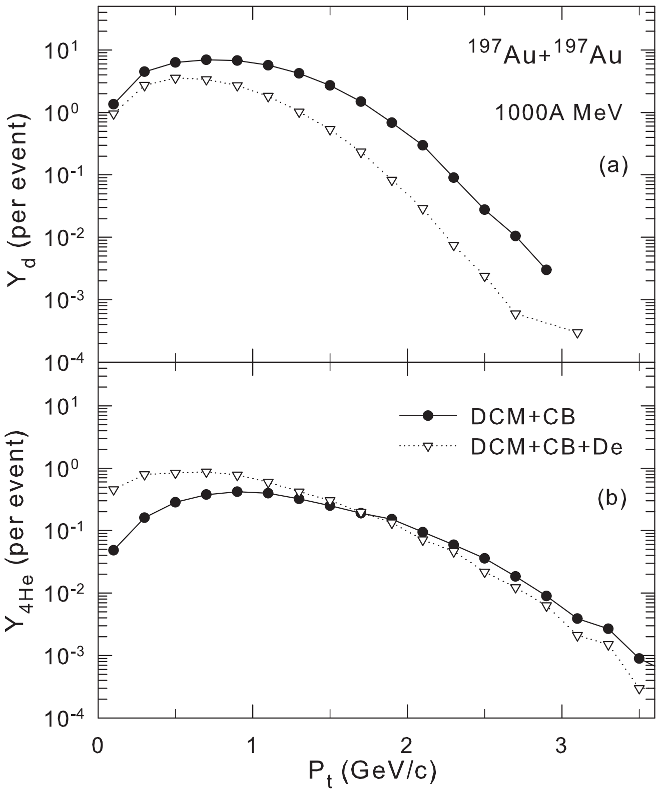

FIG. 18. Transverse momentum distribution of the coalescence clusters and final nuclei of ^{2}H (a) and ^{4}He (b). In the calculation the reaction parameters are as in Fig. 17.

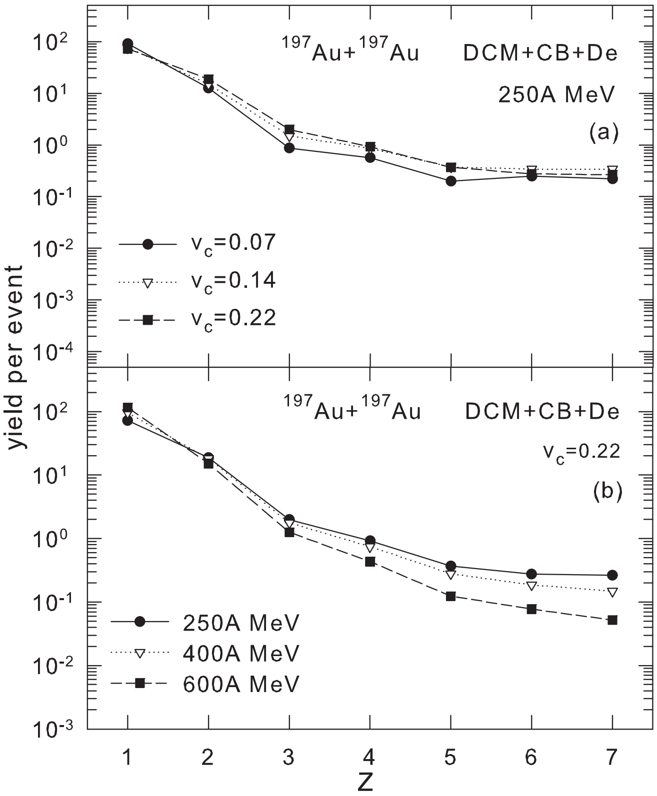

FIG. 19. Charge yields of light and intermediate mass nuclei in central collisions of two gold nuclei obtained after DCM, coalescence, and de-excitation calculations. The beam energies and the coalescence parameters are indicated in panels (a) and (b).

will follow the baryon interaction inside the diluted excited clusters.

In Fig. 21 we demonstrate the integrated charge yields extracted in the FOPI experiment with our calculations including G2 generation. We consider this kind of generation as the most adequate one for this case, since it provides very broad nucleon momentum distributions, as it could be expected in the case of realistic transport approaches (Fig. 16). For this analysis we have taken $v_c = 0.22\ c$ which gives moderate internal excitations of the primary clusters. As we have noted previously, this velocity is of the same order as the Fermi velocity inside nuclei, and provides the excitation energies around the nucleus binding energy ($\sim$10 MeV per nucleon, see Fig. 6). The total system was taken as having 394 nucleons with 158 protons (Au + Au system). Since the G2 generation is determined by the source energy we have taken the center of mass energies corresponding to the beam colliding energies. The results for the energies of 250*A* MeV and 400*A* MeV, which correspond to the center of mass energies 60*A* MeV and 95*A* MeV are shown. For more high beam energies the nuclei with $Z \gtrsim 3$ were practically not observed in the experiment. One can see a quite reasonable agreement with the data in this case. We believe, however, the involvement of other observables is necessary to get the consistent theory description.

The instructive information can be obtained by analyzing the lightest particle yields, as was shown in Figs. 13 and 14. Figure 22 presents yields of p, ^{2}H, ^{3}H, ^{3}He, and ^{4}He versus the beam energy. Within our approach we reproduce the behavior of their production as function of the energy. A very interesting experimental feature has no a reasonable explanation up to now: There is the cross-over of the ^{3}He and ^{4}He yields. At low beam energies ^{4}He dominates, while at high energy we have the standard "coalescence" situation when ^{3}He is more produced than ^{4}He. As we have pointed above (Sec. IV), the enhanced yield of ^{4}He at low energies can be naturally explained as a result of the secondary de-excitation of large primary coalescent clusters. ^{4}He formation is dominating during the statistical processes because the binding energy of ^{4}He is essentially larger than ^{3}He. However, at very high energy the primary coalescent clusters becomes rather small, therefore, the nuclei of smaller sizes have more chances to be produced. There were no attempts to explain this experimental cross-over of helium with previous theories.

Figure 23 shows the average kinetic energies of the produced nuclei. Our calculations with G2 and G3 generations do also reproduce it reasonably well. As obvious from the initial nucleon energy distributions (Fig. 1) G3 provides higher average energies for big nuclei because a lot of nucleons have high initial velocity, as a consequence a regular flow profile. However, to conclude on the nature of the flow we should look also at the full energy distributions (see Figs. 4 and 10), if they are available in experiment. We hope, in future, we will

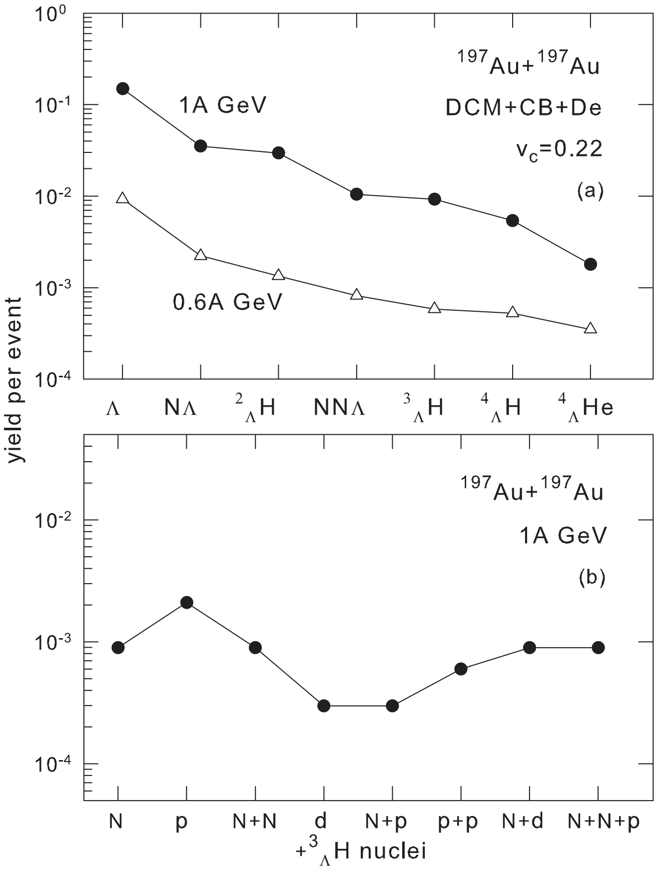

FIG. 20. Yields of hypernuclei produced in central collisions of two gold nuclei after DCM, coalescence, and de-excitation calculations. The panel (a) presents the full yields per event. The yields of correlated particles (neutrons, proton, deutrons) in channels with the $^3_\Lambda$H production are in panel (b). The beam energies are indicated in panels (a) and (b).

get such data. The result may also depend on the selection of experimental events, and this can be taken into account within our approach.

As seen from the analysis of the experimental data we have obtained the qualitative explanation for the crucial observables that was not possible to rich consistently in previous statistical and dynamical analyses of these data: (1) The yield of all nuclei can be approximately reproduced. Decreasing the large nuclei ($Z > 2$) yields with beam energy happened because of diminishing the size of primary clusters but not because of increasing the chemical temperature in the system. (2) The large kinetic energy of nuclei (flow energy) can be naturally explained by the primary kinetic motion of clusters. (3) The production of ^{4}He and ^{3}He isotopes and the cross-over of their yields can be understand as a result of the de-excitation of large primary clusters and decreasing their sizes with the beam energy. We have also verified that using DCM generator does not change this qualitative conclusion. Our consistent description of all characteristics can be considered as the confirmation of the mechanism suggested for the production of complex nuclei in central collisions.

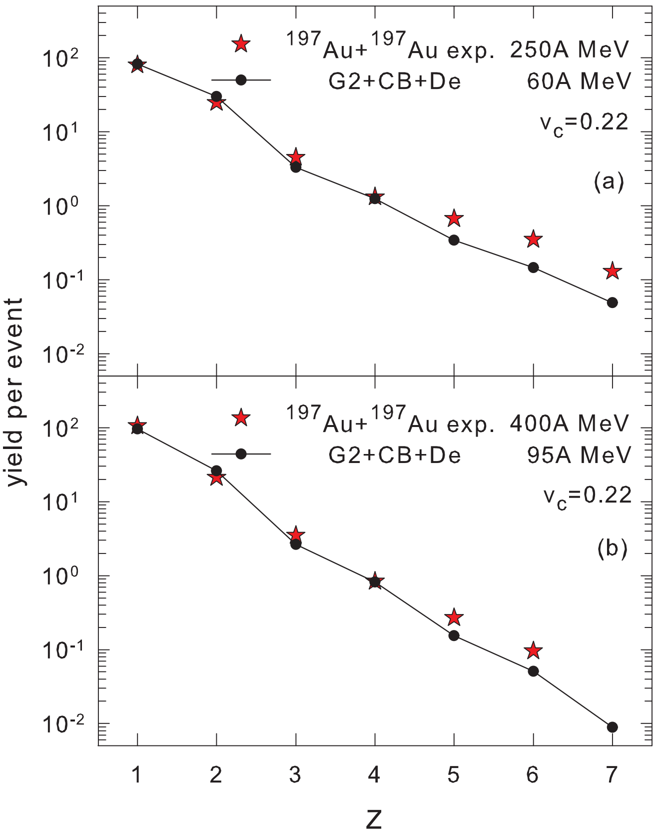

FIG. 21. Yields of nuclei versus their charge Z. The red stars are the FOPI experiment [33,34]. The parameters for the calculations including the nucleon generation in Au + Au source and source energies, coalescence and statistical de-excitation are shown in panels (a) and (b).

VII. CONCLUSION

During recent decades there is permanent increasing the number of experiments measuring nuclear reactions in central relativistic nuclear collisions. The yield of light nuclei is one of the essential observable. There is a reasonable assumption that this yield should be described by transport dynamical models if we include a relevant baryon/nucleon interactions at low energies. However, the modern transport approaches are designed mainly for the description of high-energy interactions, including both ions and hadrons ones. A sophisticated low energy nucleon interaction and other theory ingredients important for the realistic description of nuclei (e.g., the calculations of real wave functions, antisymmetrization, many-body forces, and so on) are usually beyond this scope because of complexity of this many body problem. For this reason a phenomenological coalescence approach is often used to describe the nuclei yields by assuming that the baryons are combined in the final state. This simple phenomenology disregards many aspects of low-energy collective interactions and may lead to wrong conclusions on the clusterization nature. In present our study we try to overcome the problem by considering neighbor baryons produced after the dynamical stage as clusters at certain subnuclear densities where

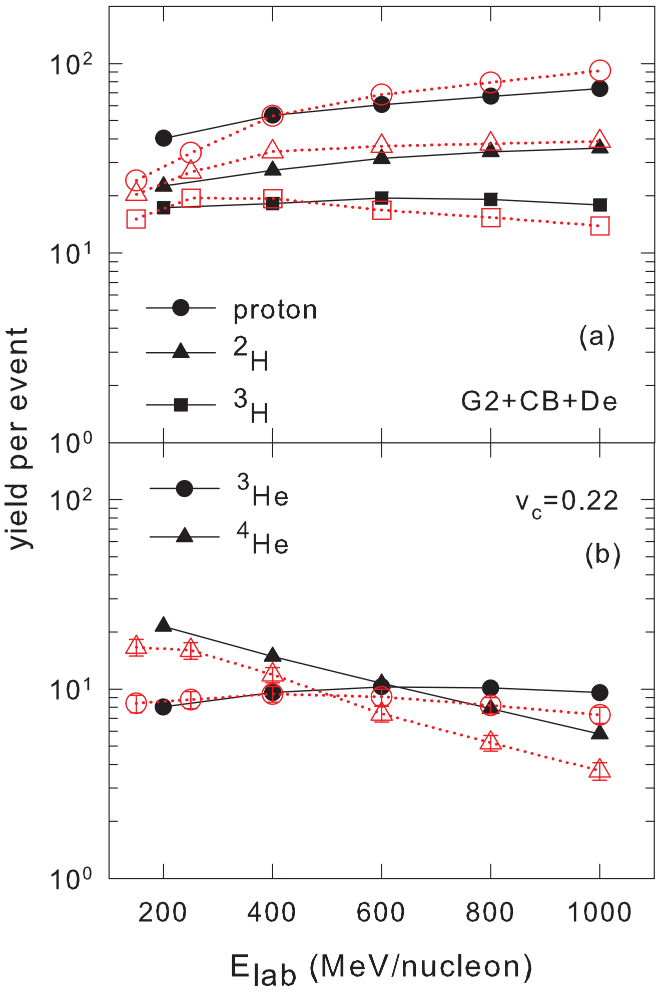

FIG. 22. Yields of lightest nuclei [noted in panels (a) and (b)] as function of the beam energy in Au + Au collisions. Red symbols connected with the dashed lines are FOPI experimental data [34]. Black symbols connected with solid lines are our (G2 + CB + De) calculations with the corresponding center of mass energies for Au + Au sources.

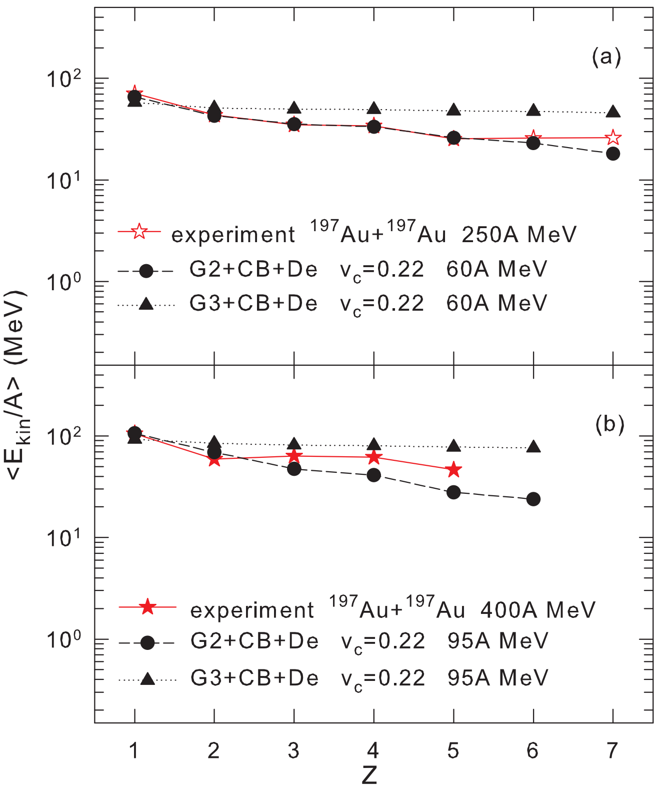

FIG. 23. Mean kinetic energy (per nucleon) of charged nuclei for central 250*A* MeV (a) and 400*A* MeV (b) of Au + Au collisions. Experimental data are in red color [34]. The parameters for our calculations (as in Fig. 21) are noted in panels (a) and (b).

the baryons are still interacting. This interaction can lead to the nuclei production and can be described in the statistical way.

In our approach, as the first step, after generating the initial baryons and their momenta, we involve the generalized coalescence model (CB) which forms big excited coalescentlike clusters. In such clusters the baryons move respect each other and interact by producing final nuclei. As we know the statistical description of such processes is commonly accepted for many physical phenomena, for example, in multifragmentation [16,17]. A crucial question is the excitation energy of such primary clusters. Namely, it determines if the finite system can be considered as an equilibrated one during the reaction. At low internal excitations the clusters' baryons are together during a long time, therefore, the thermalized conditions are fulfilled. On the contrary, at very high excitations the baryons should fly away fast, and the equilibrium criterion can be violated. Remarkably, however, that to explain the experimental data we should take the internal cluster energy of around 10 MeV per nucleon. This is close to the nuclear binding energy, and it is similar to the energy which we have previously extracted from the analysis of the projectile/target residue multifragmentation. This fact may tell us that there are common conditions for establishing equilibrium in finite nuclear systems.

We note that previously only one equilibrated excited nuclear source was assumed in the statistical models' applications for the description of nuclei production in central nucleus collisions (see, e.g., Refs. [4,16]). It might be formed as a results of the full or partial fusion of the colliding nuclei. Our approach with many such sources (i.e., excited coalescence clusters) allows for more consistent description of the reaction. The flow of the produced particles can be here explained as a dynamical motion of the clusters. The nuclei of small sizes which dominate at the very high collision energy can be now explained not as a result of very high temperatures of one source but also as a result of decreasing primary sizes of the coalescent clusters. In addition, we obtain a new physical constraint on the excitation energies of equilibrated nuclear sources of finite sizes in fast-expanded big systems.

We have theoretically investigated the main regularities of such nuclei production, in particular, charge and isotope yields, their kinetic energies. We have also investigated the influence of the initial baryon generating stage, which can be simulated by dynamical models. We can reasonably explain the recent FOPI data, however, we need new experimental data for verifying this approach. In addition to inclusive yields and energy spectra, the particle correlations and the correlated yields, which come after decay of primary hot clusters, should be the adequate observable. This mechanism allows for a new interpretation of the baryons and nuclei yields, since the secondary "statistical" interaction can change the baryon characteristics from the primary "dynamical" ones. As we found it is certainly expected in the collisions with the beam energy less than 1 GeV per nucleon. However, the higher energies are more interesting since they lead to the production of new particles and nuclei, e.g., hypernuclei. In this case we can obtain novel information on hyperons interaction at low energy in matter and new exotic species. Such kind of research can be possible at the new generation of ion accelerators of intermediate energies, as FAIR (Darmstadt), NICA (Dubna), and others. It is promising that new advanced experimental installations for the fragment detection will be available soon [43,44].

ACKNOWLEDGMENTS

The authors thank our colleagues for stimulating discussions and support of this study: J. Pochodzalla, W. Trautmann, Ch. Scheidenberger, Y. Leifels, A. Le Fevre, R. Ogul, and L. Bravina. A.S. Botvina acknowledges the support of Bundesministerium fuer Bildung und Forschung (BMBF), Germany. N.B. acknowledges the Scientific and Technological Research Council of Turkey (TUBITAK) support under Project No. 118F111. A.S.B. acknowledges the support of RFBR (Russia) according to the research Project No. 18-02-40084. M.B. and N.B. acknowledges that the work has been performed in the framework of COST Action CA15213 THOR. The authors thank the Frankfurt Institute for Advanced Studies (FIAS), J. W. Goethe University, for hospitality.

[1] J. Gosset, H. H. Gutbrod, W. G. Meyer, A. M. Poskanzer, A. Sandoval, R. Stock, and G. D. Westfall, Phys. Rev. C **16**, 629 (1977).
[2] V. D. Toneev and K. K. Gudima, Nucl. Phys. A **400**, 173 (1983).
[3] A. S. Botvina, J. Steinheimer, and M. Bleicher, Phys. Rev. C **96**, 014913 (2017).
[4] W. Neubert and A. S. Botvina, Eur. Phys. J. A **17**, 559 (2003).
[5] R. Scheibl and U. Heinz, Phys. Rev. C **59**, 1585 (1999).
[6] S. Sombun, K. Tomuang, A. Limphirat, P. Hillmann, C. Herold, J. Steinheimer, Y. Yan, and M. Bleicher, Phys. Rev. C **99**, 014901 (2019).
[7] K. Blum and M. Takimoto, Phys. Rev. C **99**, 044913 (2019).
[8] P. Kreutz *et al.*, Nucl. Phys. A **556**, 672 (1993).
[9] A. S. Botvina *et al.*, Nucl. Phys. A **584**, 737 (1995).
[10] H. Xi *et al.*, Z. Phys. A **359**, 397 (1997).
[11] R. Ogul *et al.*, Phys. Rev. C **83**, 024608 (2011).
[12] R. P. Scharenberg, B. K. Srivastava, S. Albergo, F. Bieser, F. P. Brady, Z. Caccia *et al.*, Phys. Rev. C **64**, 054602 (2001).
[13] V. E. Viola *et al.*, Nucl. Phys. A **681**, 267 (2001).
[14] L. Pienkowski, K. Kwiatkowski, T. Lefort, W.-C. Hsi, L. Beaulieu, V. E. Viola *et al.*, Phys. Rev. C **65**, 064606 (2002).
[15] V. A. Karnaukhov *et al.*, Phys. At. Nucl. **69**, 1142 (2006).
[16] J. P. Bondorf, A. S. Botvina, A. S. Iljinov, I. N. Mishustin, and K. Sneppen, Phys. Rep. **257**, 133 (1995).
[17] B.-A. Li, A. R. DeAngelis, and D. H. E. Gross, Phys. Lett. B **303**, 225 (1993).
[18] A. S. Botvina and J. Pochodzalla, Phys. Rev. C **76**, 024909 (2007).
[19] O. Hashimoto and H. Tamura, Prog. Part. Nucl. Phys. **57**, 564 (2006).
[20] J. Schaffner, C. B. Dover, A. Gal, C. Greiner, and H. Stocker, Phys. Rev. Lett. **71**, 1328 (1993).
[21] Special issue on *Progress in Strangeness Nuclear Physics*, edited by A. Gal, O. Hashimoto, and J. Pochodzalla, Nucl. Phys. A **881**, 1–338 (2012).
[22] N. Buyukcizmeci, A. S. Botvina, J. Pochodzalla, and M. Bleicher, Phys. Rev. C **88**, 014611 (2013).
[23] T. Hell and W. Weise, Phys. Rev. C **90**, 045801 (2014).
[24] A. S. Botvina, K. K. Gudima, J. Steinheimer, M. Bleicher, and I. N. Mishustin, Phys. Rev. C **84**, 064904 (2011).
[25] A. S. Botvina, K. K. Gudima, and J. Pochodzalla, Phys. Rev. C **88**, 054605 (2013).
[26] A. S. Botvina, N. Buyukcizmeci, A. Ergun, R. Ogul, and M. Bleicher, J. Pochodzalla. Phys. Rev. C **94**, 054615 (2016).
[27] A. S. Botvina, K. K. Gudima, J. Steinheimer, M. Bleicher, and J. Pochodzalla, Phys. Rev. C **95**, 014902 (2017).
[28] B. I. Abelev *et al.* (The STAR collaboration), Science **328**, 58 (2010).
[29] B. Dönigus (ALICE collaboration), Nucl. Phys. A **904-905**, 547c (2013).
[30] I. Vassiliev *et al.* (CBM collaboration), JPS Conf. Proc. **17**, 092001 (2017).
[31] NICA White Paper, http://theor0.jinr.ru/twiki-cgi/view/NICA/WebHome; https://bmn.jinr.ru/.
[32] A. S. Botvina *et al.*, Phys. Lett. B **742**, 7 (2015).
[33] W. Reisdorf *et al.*, Nucl. Phys. A **612**, 493 (1997).
[34] W. Reisdorf *et al.*, Nucl. Phys. A **848**, 366 (2010).
[35] S. A. Bass *et al.*, Prog. Part. Nucl. Phys. **41**, 255 (1998).
[36] M. Bleicher *et al.*, J. Phys. G **25**, 1859 (1999).
[37] E. L. Bratkovskaya and W. Cassing, Nucl. Phys. A **807**, 214 (2008).
[38] C. Hartnack, H. Oeschler, Y. Leifels, E. L. Bratkovskaya, and J. Aichelin, Phys. Rep. **510**, 119 (2012).
[39] Th. Gaitanos, H. Lenske, and U. Mosel, Phys. Lett. B **675**, 297 (2009).
[40] W. Neubert and A. S. Botvina, Eur. Phys. J. A **7**, 101 (2000).
[41] A. S. Lorente, A. S. Botvina, and J. Pochodzalla, Phys. Lett. B **697**, 222 (2011).
[42] T. R. Saito *et al.*, Nucl. Phys. A **954**, 199 (2016).
[43] Th. Aumann, Progr. Part. Nucl. Phys. **59**, 3 (2007).
[44] H. Geissel *et al.*, Nucl. Inst. Meth. Phys. Res. B **204**, 71 (2003).